



Acoustic emission and damage characteristics of granite under graded cyclic loading

Shengjun Miao¹ · Daohong Xia¹ · Pengjin Yang¹ · Mingchun Liang¹

Received: 22 October 2021 / Accepted: 21 April 2022 / Published online: 11 May 2022
© Saudi Society for Geosciences 2022

Abstract

A graded cyclic loading test was designed and conducted. The mechanical characteristics, acoustic emission (AE), and energy evolution law of granite under cyclic loading were demonstrated. Meanwhile, a multifactor damage model of granite under graded cyclic loading was constructed. Results indicated that hysteresis evidently existed in the stress–strain curve of granite. The envelope curve consisted of compaction, elastic, yield, failure, and residual strength stages. The Poisson's ratio of granite was minimally affected by cyclic loading and confining pressure. Conversely, the elastic modulus of granite was highly sensitive to cyclic loading and confining pressure. Considerable AE phenomena occurred in the yield and failure stages. After entering the residual strength stage, the AE intensity of granite decreased until it disappeared. In the cycle process, the proportion of elastic energy is higher than that of dissipated energy. As the number of cycles increased, the elastic energy proportion and dissipated energy proportion increased and decreased, respectively; finally, both tended to be stable. The damage state of granite during the cyclic loading test was quantitatively described by the newly established multifactor damage model. The damage degree of granite under graded cyclic loading was mainly determined by loading stress level.

Keywords Granite · Graded cyclic loading · Acoustic emission · Energy evolution · Damage model

Introduction

In the construction and operation stages of geotechnical engineering, such as tunnel blasting excavation, the operation stage of roads and bridges, the storage and drainage processes of reservoir dams, and the injection and production processes of gas, cyclic loading is often encountered. As a kind of heterogeneous natural material, a rock contains

substantial cracks and pores, which makes the rock show anisotropic and nonlinear characteristics under loading (Bieniawski 1967). Microcracks will also be generated under loading for intact rocks, which is the reason for the nonlinear mechanical characteristics (Wei et al. 2021; Manogharan et al. 2021). The above characteristics make the mechanical properties of rocks under cyclic loading significantly different from those under conventional loading (Heap et al. 2009; Zhu et al. 2018; Xu et al., 2004). Rock damage is also nonlinear due to cyclic loading, which will affect the stability of geotechnical and underground engineering in long-time operation (Liu et al. 2016; Miao et al. 2021). Therefore, rock mechanical and damage characteristics under cyclic loading should be researched.

Some scholars have analysed the variation in rock strength, deformation characteristics, and mechanical parameters under cyclic loading (Singh and Naidu 2001; Bagde and Petros 2005; Wang et al. 2013; Guo et al. 2018). With the deepening of the research, new technical methods have been applied to study rocks under cyclic loading. Specifically, acoustic emission (AE) technology could capture elastic waves to determine internal fracture changes in rock materials (Falmagne et al. 1998; Thompson et al., 2006). On this

Responsible Editor: Zeynal Abiddin Erguler

✉ Daohong Xia
xiadaohong_737@163.com

Shengjun Miao
miaoshengjun@ustb.edu.cn

Pengjin Yang
ypj12523@163.com

Mingchun Liang
lmch1993@outlook.com

¹ Beijing Key Laboratory of Urban Underground Space Engineering & School of Civil and Resource Engineering, University of Science and Technology Beijing, Beijing 100083, China

basis, Trippetta et al. (2013) researched the stress condition and AE events of rocks during earthquakes. They found that the mechanical variation of rocks at different cycle stages can be identified using AE data. Zhang et al. (2018) performed uniaxial cyclic loading for rocks and demonstrated the relationship between AE events and failure behaviour. From a post-peak cyclic loading test, Tang et al. (2020a) identified that “*b*” value and AE number were highly sensitive to rock crack propagation under post-peak cyclic loading. In accordance with digital image correlation, they also found that a high loading rate can inhibit the development of the crack tip for granite during cyclic loading (Tang et al. 2020b). Zhao et al. (2020) obtained failure precursor information of sandstone with different water contents under various upper limit cyclic loading tests via AE technology. Chen et al. (2021) divided the fracture process of saturated tuff under different confining pressures by AE events, mainly including microcrack initiation, microcrack propagation, and macrocrack formation stages. Wang et al. (2021a, b) determined the rapid damage initiation point of tuff under triaxial loading–unloading in accordance with lag energy and AE signal.

The first law of thermodynamics shows that rock failure and rock damage must be accompanied by energy conversion (Mikhalyuk and Zakharov 1997; Sujathal and Kishen, 2003; Xie et al. 2008). Some scholars have elaborated their characteristics under cyclic loading through energy evolution. Through a uniaxial cyclic loading test of sandstone, Meng et al. (2016) found that before the cyclic load reached the peak stress, the energy mainly accumulated inside the rock. Zhang et al. (2017) analysed the influence of confining pressure on rock energy density by changing the confining pressure in cyclic loading test. Gao and Feng (2019) found via a true triaxial cyclic loading test of marble that rock damage was anisotropic and that the change in dissipated energy with equivalent irreversible strain was linear. Li et al. (2019) demonstrated the mechanism of energy evolution in the process of rock failure via two groups of cyclic loading tests. Through cyclic loading tests on three types of rock samples, Song et al. (2020) quantitatively studied the change in energy density during uniaxial loading.

The above scholars studied the deformation and damage characteristics of rocks under cyclic loading from the perspective of AE and energy. However, the upper limit loading of cyclic loading test in these studies is mostly constant. In practical engineering, the cyclic loading in geotechnical engineering cannot be constant; that is, the loading stress level of each cycle is different. Therefore, some scholars have also studied the deformation failure and AE characteristics of rocks under graded cyclic loading. Zhu et al. (2016) and Shen et al. (2022) found that coal rocks were mainly in the form of shear failure under grade cyclic loading. Meng et al. (2018) analysed the characteristics of crack development and the law of AE events in rocks in the grade cyclic loading test. Fu et al. (2016) found that when marble was subjected to graded cyclic loading, the

AE events have obvious segmentation characteristics. Additionally, some innovative results about the energy evolution and distribution law of rocks under graded cyclic loading were obtained (Wu et al. 2020; Meng et al. 2020; Shen et al. 2022). Almost majority of these pieces of research focussed on revealing the results and regularity of the tests, but they overlooked the performance of rocks in terms of damage and the research on theoretical improvement. Moreover, most of the research results were obtained based on uniaxial graded cyclic loading tests, and many conclusions were not applicable to the case of triaxial loading. On this basis, with granite as the test and research object, uniaxial and triaxial graded cyclic loading models were designed to make the test close to practical engineering in some cases. Then, the mechanical properties and deformation failure characteristics under cyclic loading were analysed through AE phenomenon and energy. Afterwards, a multifactor damage model considering confining pressure and loading stress level was established to describe the damage state of granite during graded cyclic loading quantitatively.

Design of test scheme

The granite used in this test was collected from the Jinyuan mining area in Lingbao City, Henan Province, China. The specimens (50 mm in diameter and 100 mm in height) were made in conformity to the *Standard of the International Society for Rock Mechanics*. The P-wave velocity of the specimens was measured using ZBL-U5200 ultrasonic detection equipment, and the specimens with a P-wave velocity of 4000–4100 m/s were selected for the test to decrease the discreteness of specimens. The MTS-815 testing machine in the University of Science and Technology Beijing was used as a loading device. The test systems consisted of axial pressure, confining pressure, and AE systems (Fig. 1). The AE system and the

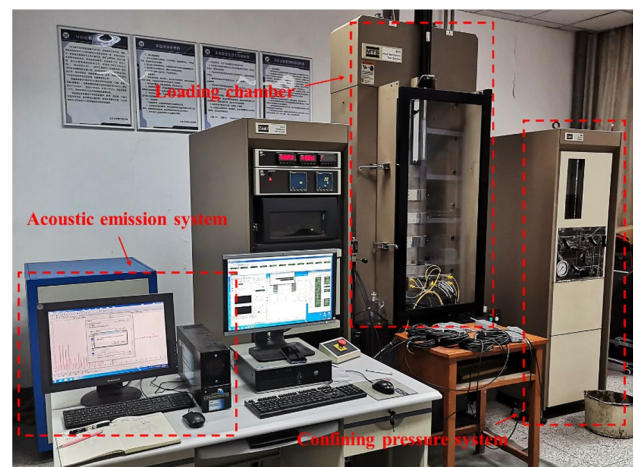


Fig. 1 MTS-815 rock test system

installation of AE sensors are shown in Fig. 2. The resonant frequency of the AE system was 140 kHz, and the threshold noise value and main amplifier gain were both 40 dB. The sampling frequency of the AE system was set to 1 M times/s. The loading was controlled by axial force. The loading and unloading rates were set to 0.6 kN/s, which could not only ensure the test efficiency but also prevent the impact damage of specimens. Triaxial compression tests were conducted before cyclic loading tests to determine the upper limit of axial force per cycle, and the test results are shown in Fig. 3. Figure 3 indicates that the peak stresses of granite under confining pressures of 0, 10, 20, and 30 MPa were 90.52, 242.18, 281.92, and 340.92 MPa, respectively. To ensure that the rock sample was not seriously damaged during cyclic loading and that the internal energy evolution characteristics could be reflected, the upper limit stresses of the first loading and the fifth loading were controlled at approximately 20% and 70% of the peak stress, respectively. On this basis, the stress path of graded cyclic loading tests of granite was obtained, as shown in Fig. 4. The values of upper limit axial force under different cycles are shown in Table 1. Triaxial cyclic loading tests were performed with five rock samples under each confining pressure to reduce the test error. The results of the five tests have similar laws. In consideration of the limitation in paper quantity, results of only one representative test under each confining pressure were presented.

Mechanical test results of granite under graded cyclic loading

Stress–strain curve

The failure modes and stress–strain curves of granite are shown in Fig. 5. On the basis of Fig. 5, the following

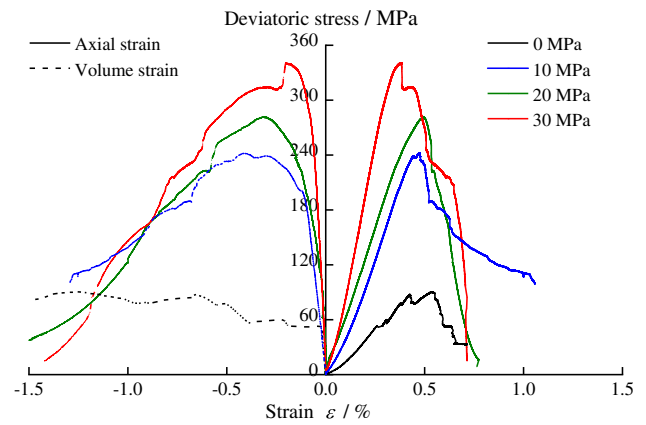


Fig. 3 Complete stress–strain curve under different confining pressures

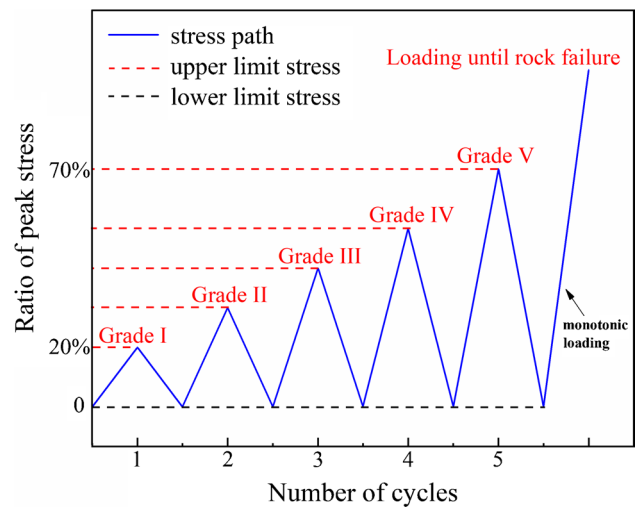


Fig. 4 Stress path of graded cyclic loading tests

Fig. 2 Installation of acoustic emission sensors

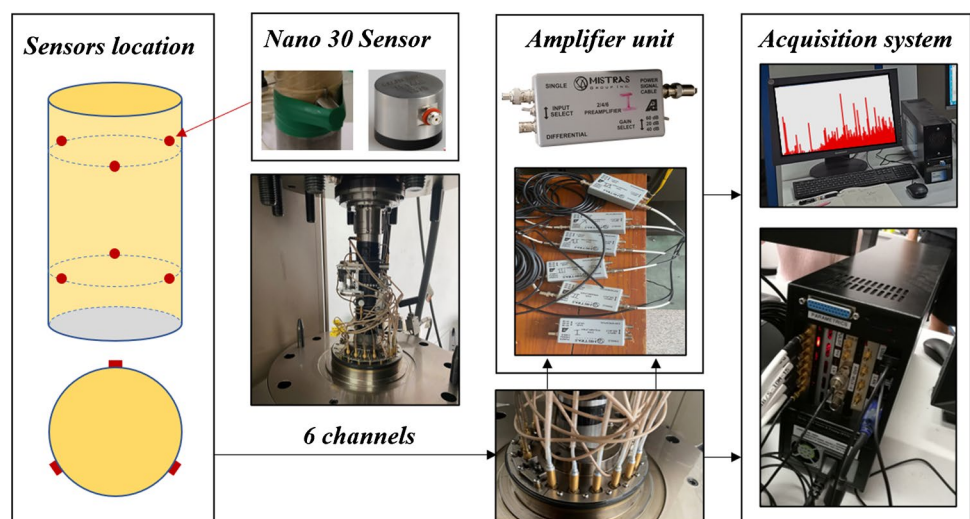


Table 1 Values of upper limit axial force under different cycles (kN)

Confining pressure	Upper limit axial force				
	Cycle 1	Cycle 2	Cycle 3	Cycle 4	Cycle 5
0	30	50	70	90	120
10	80	120	170	230	300
20	150	190	240	300	390
30	160	210	270	340	420

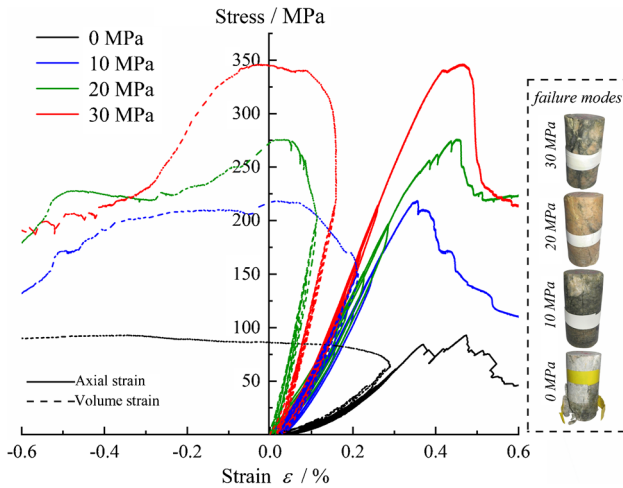


Fig. 5 Stress–strain curves and failure modes under different confining pressures

results were found: (1) The shape of the envelope curve under cyclic loading can be divided into compaction stage, elastic stage, yield stage, failure stage, and residual strength stage. (2) From the view of failure modes, the rock samples under the four confining pressures are single-fracture surface failure. The rock samples under triaxial cyclic loading maintain high integrity. On the contrary, the failure of rock samples under uniaxial (the confining pressure is 0 MPa) cyclic loading produces a small amount of fragments. (3) Compared with the characteristics of the compaction stage under triaxial cyclic loading, the compaction stage under uniaxial cyclic loading accounts for a larger proportion, and the stress–axial strain curve of residual strength fluctuates more rapidly. This phenomenon is also reflected in the relationship between stress and volume strain. Confining pressure exerts a restrictive effect on the post-peak morphology of the two kinds of stress–strain curves. (4) The stress–axial strain curves and the stress–volume strain curves show a hysteresis effect, which forms stress–strain hysteresis loops. The reason for this phenomenon is that microcracks are present in the rock, which is not an ideal elastic material. When the unloading is performed after the stress reaches a certain value, a hysteresis effect occurs in the recovery of

strain, and the strain generated during loading is not fully recovered during unloading. (5) The area of the hysteresis loop stands for the energy loss of rock samples during cyclic loading. When the load level under each confining pressure does not reach the peak stress, the stress–axial strain curves are closely distributed, which means that the hysteresis loop area is small. The energy loss of granite is proved small under cyclic loading (Guo et al. 2018; Vaneghi et al. 2020; Wang et al., 2021a, b). (6) The confining pressures of this cyclic loading test are 0, 10, 20, and 30 MPa, and the corresponding peak stresses are 92.97, 218.46, 275.90, and 346.19 MPa, respectively. With the increase in confining pressure, the volume dilatancy stress of granite also increases. Meanwhile, the influence of confining pressure on peak stress is evident. The reason is that confining pressure can limit the lateral deformation and improve the bearing capacity of the rock sample.

Elastic modulus and Poisson’s ratio

In these cyclic loading tests, the elastic modulus is calculated using the following formula:

$$E_i = \frac{\Delta\sigma(i)}{\Delta\varepsilon_a(i)} \tag{1}$$

The Poisson’s ratio can be obtained as follows:

$$\nu_i = \frac{\Delta\varepsilon_r(i)}{\Delta\varepsilon_a(i)} \tag{2}$$

where $\Delta\sigma(i)$ is the difference between the upper limit stress and the lower limit stress during the i -th loading or unloading; $\Delta\varepsilon_a(i)$ is the difference between the axial strain at the upper limit stress and the axial strain at the lower limit stress during the i -th loading or unloading; $\Delta\varepsilon_r(i)$ is the difference between the transverse strain at the upper limit stress and the transverse strain at the lower limit stress during the i -th loading or unloading.

The calculations are shown in Table 2. Table 2 presents the following results: (1) When the confining pressure is constant, as the number of cycles increases, the elastic modulus of granite first increases and then tends to be stable. By contrast, the Poisson’s ratio is almost unchanged. When the number of cycles is constant, the elastic modulus and Poisson’s ratio in the unloading stage are slightly higher than those in the loading stage. (2) When the number of cycles is constant, as the confining pressure enhances, the elastic modulus of granite increases significantly. Confining pressure has a distinct impact on improving the elastic modulus of granite. (3) When the number of cycles is constant, the Poisson’s ratio of the granite sample increases slightly when the confining pressure is applied. The enhanced confining pressure and cyclic loading have a minimal effect on Poisson’s ratio.

Table 2 Results of elastic modulus and Poisson’s ratio of rock samples

Confining pressure/MPa	Number of cycles	1↑	1↓	2↑	2↓	3↑	3↓	4↑	4↓	5↑	5↓
0	<i>E</i> /GPa	38.97 (7.9%)	53.23 (10.2%)	56.97 (−3.5%)	58.60 (−6.4%)	60.03 (8.2%)	61.34 (2.1%)	62.34 (10.2%)	63.55 (6.7%)	63.97 (−6.0%)	64.78 (9.0%)
	ν	0.145 (10.0%)	0.158 (7.1%)	0.132 (6.6%)	0.142 (5.3%)	0.135 (7.2%)	0.141 (4.5%)	0.138 (−4.7%)	0.151 (9.1%)	0.142 (1.0%)	0.151 (−7.4%)
10	<i>E</i> /GPa	43.49 (6.3%)	54.69 (5.6%)	57.18 (8.3%)	58.83 (4.6%)	61.52 (−3.3%)	65.69 (9.6%)	66.98 (8.9%)	67.49 (−5.3%)	68.86 (−4.1%)	69.69 (3.9%)
	ν	0.164 (8.2%)	0.177 (8.1%)	0.168 (−4.6%)	0.188 (−2.9%)	0.158 (7.0%)	0.164 (9.1%)	0.162 (11.7%)	0.176 (7.5%)	0.164 (9.0%)	0.171 (10.3%)
20	<i>E</i> /GPa	54.36 (−2.9%)	63.59 (5.1%)	68.63 (11.8%)	69.81 (8.7%)	69.96 (6.8%)	70.33 (8.0%)	70.26 (6.5%)	70.78 (−1.9%)	71.2 (2.4%)	71.32 (9.5%)
	ν	0.165 (5.5%)	0.171 (9.2%)	0.177 (7.2%)	0.186 (7.5%)	0.168 (10.1%)	0.174 (−7.0%)	0.168 (8.4%)	0.179 (7.2%)	0.162 (11.2%)	0.169 (−4.7%)
30	<i>E</i> /GPa	64.21 (−2.3%)	80.38 (6.2%)	83.43 (6.3%)	84.24 (−1.0%)	87.55 (3.4%)	89.79 (−5.2%)	91.97 (5.0%)	92.64 (6.8%)	93.02 (8.2%)	93.38 (−4.5%)
	ν	0.166 (10.1%)	0.170 (8.9%)	0.159 (10.1%)	0.168 (7.2%)	0.164 (−6.6%)	0.184 (11.9%)	0.165 (13.6%)	0.173 (8.57%)	0.169 (−1.1%)	0.176 (−2.9%)

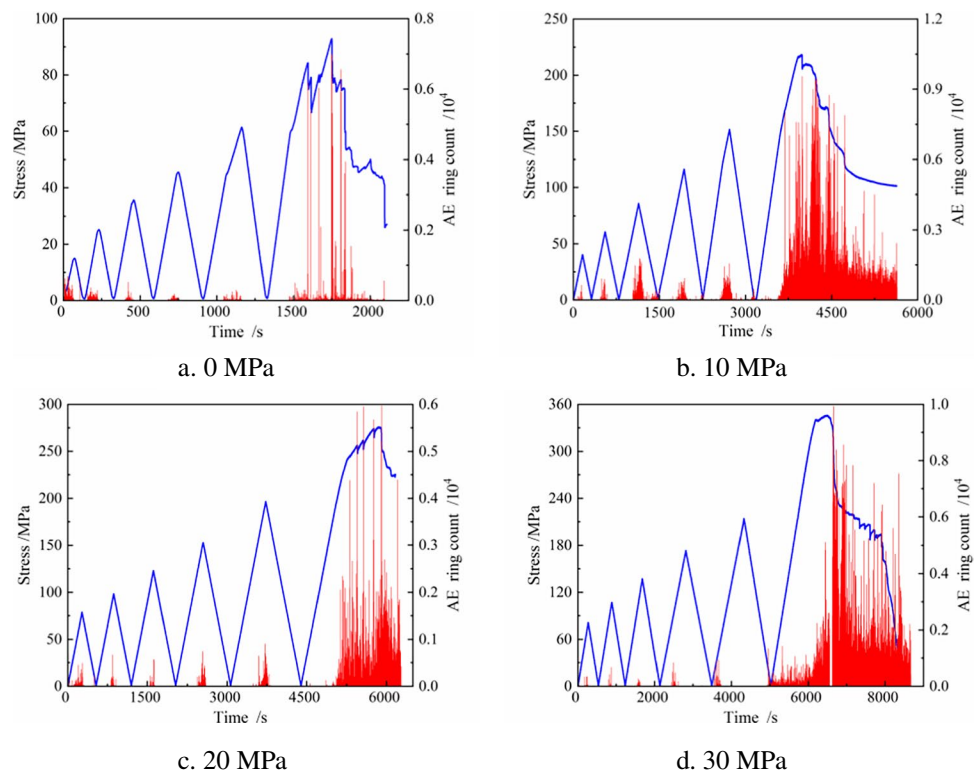
↑ denotes loading process; ↓ denotes unloading process. The error between this value and the average value is in parentheses

AE characteristics of granite under cyclic loading

The test results of AE are shown in Fig. 6. The results are detailed as follows: (1) The variation laws of AE ringing

count under different confining pressures are similar for the triaxial cyclic loading test. Firstly, when the stress reaches the upper limit loading at the cyclic loading stage, a small number of AE events occur in the rock, and almost no AE energy is released. The reason is that microcracks are compacted and closed by confining pressure and axial load. When the stress

Fig. 6 Results of acoustic emission ring count



value is considerably below the upper limit loading, almost no AE event occurs in the rock, which proves the existence of the Kaiser effect. Secondly, when stress is at a low level, almost no AE event occurs in the rock at the monotonic loading stage. As the load level approaches the peak stress, an inflection point exists in the stress–time curve, which indicates that the curve enters into the yield stage. In this stage, the number of AE ring counts increases sharply, which can reach 5–10 times of that in the cyclic loading stage. It indicates that the internal microcracks begin to produce and continue to develop because of the influence of increased load levels. This AE phenomenon can be regarded as a forerunner to estimate the rock failure. Thirdly, when the stress in the monotonic loading stage reaches the peak stress, the rock is broken, and the curve enters the failure stage. In this stage, the AE index remains at a high level. Every fracture of rock is accompanied by high energy release. Finally, the curve enters the residual strength stage over time. In this stage, the load begins to decrease slowly, and the AE events decrease evidently, which indicates that the failure of rock structure caused by stress is basically completed. (2) Under uniaxial cyclic loading, many AE events occur at the beginning of the first cycle, which is different from the phenomenon under triaxial cyclic loading. The reason for the difference is that under uniaxial cyclic loading, the stress concentration phenomenon occurs on the specimen surface due to the lack of restraint by confining pressure. In addition, the laws of AE of other stages under uniaxial cyclic loading are basically consistent with those under triaxial cyclic loading.

Damage evolution of granite under graded cyclic loading

Energy variation characteristics

The stress–strain curve has a hysteretic effect in the form of energy dissipation during cyclic loading of granite. The axial load does work on the specimen, and the specimen absorbs energy due to the axial compression deformation in the loading process. One part of the absorbed energy is translated into elastic energy, and the other part is consumed by plastic deformation and other behaviours of the rock. The plastic deformation energy, kinetic energy, friction heat energy, and radiation energy are collectively referred to as dissipated energy. Given that other forms of energy account for an extremely small proportion, the dissipated energy in this paper only considers the plastic deformation energy. The two kinds of energy can be determined from Fig. 7.

The total amount of material energy keeps constant during transferring, which is stated by the first law of thermodynamics. The formula is as follows:

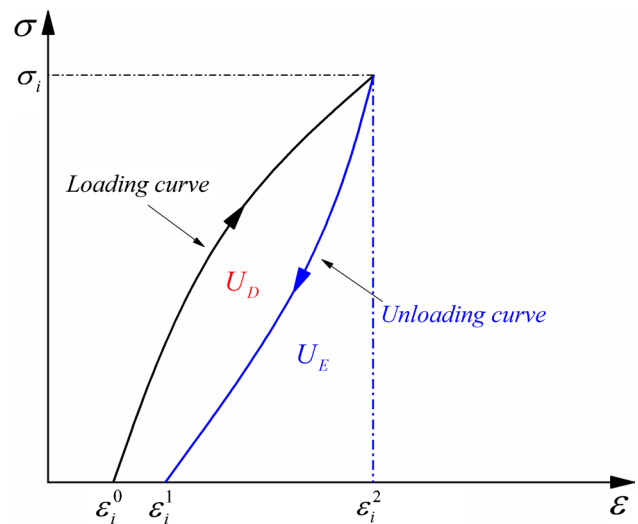


Fig. 7 Schematic diagram of energy calculation

$$U_A = U_E + U_D \tag{3}$$

where U_A is the total energy density; U_E is the elastic energy density; U_D is the dissipated energy density. The total energy density during the i -th cyclic loading and unloading is obtained using the following formula:

$$U_A = \int_{\epsilon_i^0}^{\epsilon_i^1} \sigma_i d\epsilon \tag{4}$$

where ϵ_i^0 is the initial strain of the i -th cyclic loading; ϵ_i^1 is the final strain of the i -th cyclic loading (the initial strain of the i -th cyclic unloading); σ_i is the upper stress of the i -th cyclic loading. The elastic energy density during the i -th cyclic loading and unloading is obtained using the following formula:

$$U_E = \int_{\epsilon_i^1}^{\epsilon_i^2} \sigma_i d\epsilon \tag{5}$$

where ϵ_i^2 is the final strain of the i -th cyclic unloading. Through combining Eqs. (3)–(5), the calculation formula for dissipated energy density during the i -th cyclic loading and unloading is obtained as follows:

$$U_D = \int_{\epsilon_i^0}^{\epsilon_i^1} \sigma_i d\epsilon - \int_{\epsilon_i^1}^{\epsilon_i^2} \sigma_i d\epsilon \tag{6}$$

Figure 8 shows the calculation results. We obtain the following findings: (1) The average growth rates of the two kinds of energy density are approximately 1 and 0.2 kJ/(m³•MPa). The average growth rate of dissipated energy density is much smaller than that of elastic energy density. The reason is that the internal cracks of

the specimen are closed by extrusion and then kept in an equilibrium state. In this case, the elastic energy is dominant, which is stored in the specimen. (2) Under the same load level, the two kinds of energy density decrease evidently when the confining pressure is applied to the specimen. This result indicates that few cracks exist in the rock and that confining pressure can limit the generation of rock fractures.

The proportion change curves of the two kinds of energy are also shown in Fig. 8, and the following findings are acquired: (1) The elastic energy proportion of granite is more than 0.65, whereas the dissipated energy proportion is less than 0.35, which shows that most of the input energy is converted into elastic energy when the upper limit loading under cyclic loading process is below 70% of the peak stress. (2) As the stress increases, the elastic energy proportion shows a slight upward trend and then remains stable, whereas the proportion of dissipated energy shows a slight downward trend and then remains stable. Hence, the energy conversion of granite has been completed before the stress reaches the peak stress. (3) The confining pressure can change the energy distribution of rock, which mainly shows that as the confining pressure enhances, the dissipated energy proportion decreases and the elastic energy proportion increases. Corresponding to practical engineering, when the original rock stress is enormous, the elastic energy proportion is high. At this moment, if engineering excavation is conducted, substantial elastic energy will be released, which can easily cause engineering accidents. This factor is also the main reason for the frequent occurrence of rockburst disasters in the process of deep engineering mining.

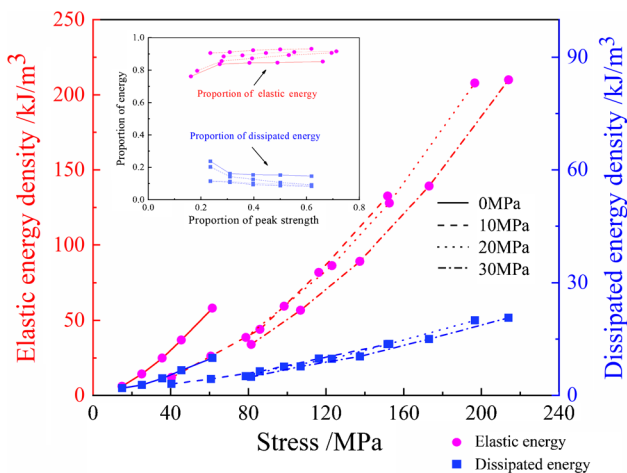


Fig. 8 Evolution curves under different confining pressures

Multifactor damage model based on energy evolution

Establishing a rock damage model is an effective and reliable method to study the damage development of a rock during cyclic loading quantitatively. Studies have shown that when the damage variables are defined by elastic modulus, plastic strain or other parameters in traditional methods, negative damage will occur at the initial loading stage due to the original defects and nonlinear characteristics of the rock. This characterisation method is inconsistent with the actual situation. Considerable research has shown that when a rock is damaged and destroyed during cyclic loading, the absorption and release of energy will occur simultaneously. When the loss of kinetic energy and frictional heat energy in the rock is ignored, the dissipation energy is only related to the rock damage and failure. Hence, the ratio of dissipated energy can define the rock damage condition. The formula of damage variable D_i of rock after i -th cycle is as follows:

$$D_i = \frac{\sum_1^i U_D}{\sum_1^n U_D} \tag{7}$$

where $\sum_1^i U_D$ is the accumulation of dissipated energy from the first cycle to the i -th cycle; $\sum_1^n U_D$ is the accumulation of dissipated energy from the first cycle to rock failure. When the stress is loaded to the peak stress, the rock will be destroyed. The rock reaches the state of complete damage at this moment, and the damage variable $D = 1$. The maximum cyclic upper limit loading in this test is only 70% of the peak stress, which does not reach the peak stress point during the cyclic process. Equation (5) is difficult to use to calculate the elastic energy from the end of the last cyclic unloading to the peak stress point. Liu et al. (2020) proposed a method to calculate the instantaneous elastic energy by using elastic modulus. The formula is as follows:

$$U_{Et} = \frac{\sigma_{it}^2}{2E_t} \tag{8}$$

where σ_{it} is the instantaneous stress; E_t is the instantaneous modulus of elasticity. The elastic energy at the peak stress point can be considered the entire elastic energy of the rock during the last monotonic loading, and it can be calculated using Eq. (8). Through substituting the result of Eq. (8) into Eq. (3), the dissipated energy of the rock during the last monotonic loading can be obtained.

The initial damage variable of granite is regarded as 0, and the damage variable at the peak stress is considered 1. The calculation results of rock damage variables are shown in Table 3. Meanwhile, the damage variable values under different numbers of cycles and loading stress levels

Table 3 Calculation results of granite damage variables

Confining pressure/MPa	Number of cycles				
	1	2	3	4	5
0	0.010	0.020	0.033	0.046	0.071
10	0.011	0.023	0.055	0.092	0.154
20	0.017	0.033	0.055	0.102	0.168
30	0.025	0.045	0.075	0.114	0.171

are presented in Fig. 9. The damage variable of granite increases gradually with the increase in the number of cycles and loading stress level. When the confining pressure increases, the damage variable of granite increases at the same cycle times, as depicted in Fig. 9. However, the mechanical test results show that confining pressure can inhibit granite damage under cyclic loading. The reason for this phenomenon is that when the confining pressure increases, the loading stress level at the same cycle times increases, resulting in intensified damage to granite. Accordingly, the major factor of granite damage during cyclic loading test is the stress level. The fact that the damage variable does not exceed 0.20 also shows that the damage of granite is minimal in five cycles, which is due to the low loading stress level. The yield stage of granite does not reach the low loading stress level, and the internal structure of the granite is not seriously damaged. This phenomenon is consistent with the results from mechanical tests.

On the basis of the calculation results of damage variables, a three-dimensional damage surface of granite under graded cyclic loading is constructed using an interpolation method, as shown in Fig. 10. The damage variable evolution characteristics of granite can be obtained from Fig. 10. With the increase in loading stress level, the

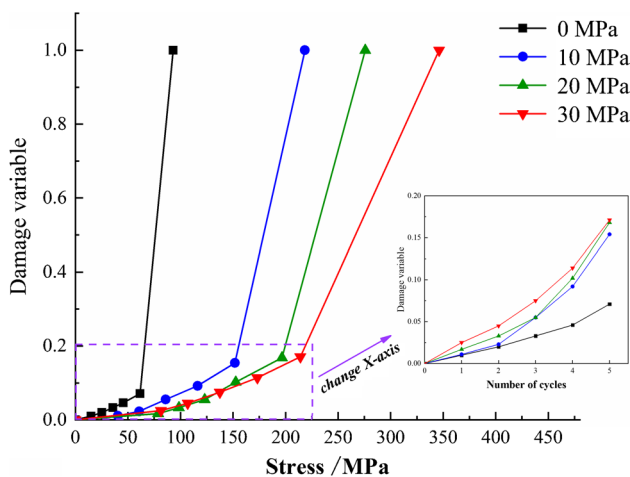


Fig. 9 Damage variable values evolution law

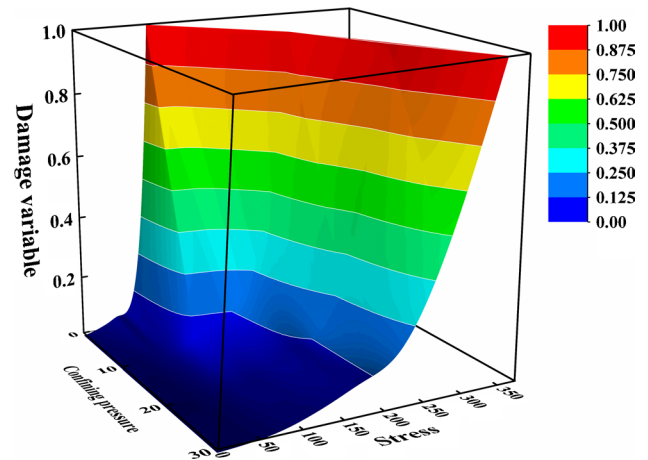


Fig. 10 Damage surface of granite under cyclic loading

granite damage increases. When the loading stress level makes the granite enter the yield stage, the granite damage rises significantly. Furthermore, with the increase in confining pressure, the slope of the damage surface of the granite under a low loading stress level becomes smaller, which indicates that confining pressure can inhibit the damage of the granite.

To describe the damage surface quantitatively, the damage variable formula is defined as

$$D = \frac{A}{10,000} \times \left(\frac{\sigma}{B}\right)^C \tag{9}$$

where D is the damage variable; σ is the loading stress during the test; A , B , and C are the parameters related to confining pressure.

The calculation results for damage variables in Table 3 are fitted using Eq. (9), and the fitting results are shown in Fig. 11. The fitting correlation coefficients of damage variables under four confining pressures are more than 0.96, indicating that the fitting results are considerably close to the calculation results. The values of A , B , and C under different confining pressures are shown in Table 4. Meanwhile, Fig. 12 illustrates the fitting results of three parameters about confining pressure. The relationship between A , B , and C and confining pressure is logarithmic, linear, and logarithmic, respectively. The fitting correlation coefficients of parameters are above 0.99, which indicate a great fitting effect. The fitting formulas are as follows:

$$A = 1.126 \ln(\sigma_p + 1.424) + 1.849 \tag{10}$$

$$B = 0.196\sigma_p + 18.000 \tag{11}$$

$$C = -0.418 \ln(\sigma_p + 0.116) + 4.208 \tag{12}$$

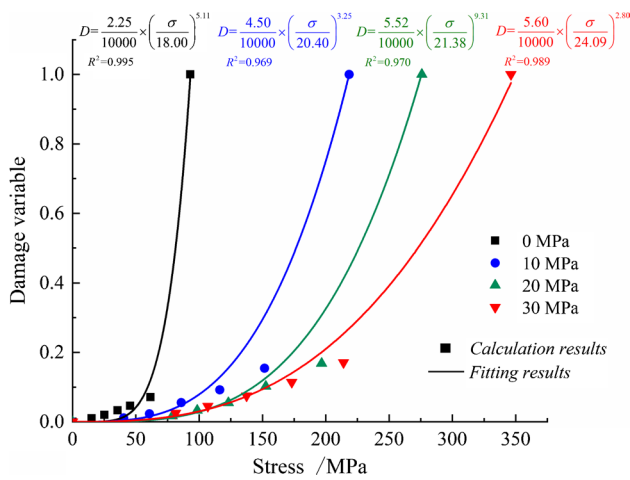


Fig. 11 Fitting results of damage variable under different confining pressures

Table 4 Parameter values under different confining pressure

Confining pressure/MPa	Parameters		
	A	B	C
0	2.25	18.00	5.11
10	4.50	20.40	3.25
20	5.52	21.38	2.93
30	5.60	24.09	2.80

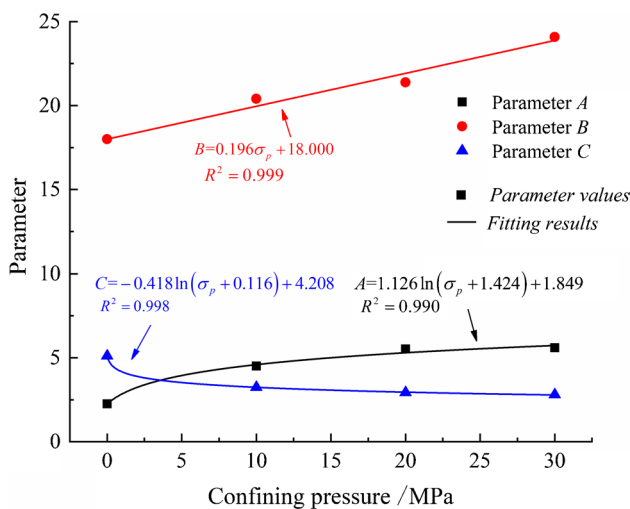


Fig. 12 Fitting results of parameter about confining pressure

where σ_p is the confining pressure (unit: MPa). Thus, the multifactor damage model of granite under graded cyclic loading test has been established. When confining pressure and loading stress level are given, the values of A, B,

and C can be calculated using confining pressure through Eqs. (10)–(12). Then, the damage variable of granite can be obtained by substituting the calculation results into Eq. (9) and inputting loading stress, which can be used to evaluate the damage state of the granite.

Conclusions

A graded cyclic loading test is designed. The laws of deformation and failure for granite during cyclic loading are explored through graded cyclic loading tests and AE monitoring. The damage variable of the rock under cyclic loading is defined by energy. A multifactor damage model considering confining pressure and loading stress level is established. The conclusions are as follows:

- (1) Under uniaxial and triaxial cyclic loading, the stress–strain curves of granite show an evident hysteretic effect. The envelope curve consists of compaction, elastic, yield, failure, and residual strength stages. Cyclic loading has minimal impact on the peak stress, whereas confining pressure can significantly improve the peak stress of granite.
- (2) The elastic modulus of granite increases slightly at first and then remains unchanged under cyclic loading. The elastic modulus at the loading stage is slightly smaller than that at the unloading stage. As confining pressure enhances, the elastic modulus of granite increases. The Poisson’s ratio of granite is inconsiderably affected by the cyclic loading and almost remains unchanged during the entire test.
- (3) Under the monotonic loading stage, when the stress is close to the peak stress, the AE events increase sharply. Then, the number of AE events remains at a high level. When entering the residual strength stage, the AE events begin to decrease evidently. Under uniaxial cyclic loading, the AE phenomenon of granite occurs at the initial phase of the first loading, which is related to the stress concentration on the granite surface. Confining pressure can reduce the amount of AE of granite.
- (4) The dissipated energy proportion of granite is lower than the elastic energy proportion. As stress enhances, the elastic energy proportion and dissipated energy proportion show the trends of “increase first and then stabilise” and “decrease first and then stabilise”, respectively.
- (5) The newly established damage model can consider both confining pressure and loading stress level. Meanwhile, the multifactor damage model has a high fitting correlation, which indicates that the damage state of granite during graded cyclic loading test can be accurately described by the model. The loading stress level is the

main reason for the granite damage in the cyclic loading test.

Acknowledgements This work was supported by the National Natural Science Foundation of China (Nos. U2034206, 51974014, and 51574014) and the National Key Research and Development Project (2018YFC0604601).

Declarations

Conflict of interest The authors declare that they have no competing interests.

References

- Bagde MN, Petros V (2005) Fatigue properties of intact sandstone samples subjected to dynamic uniaxial cyclical loading. *Int J Rock Mech Min* 42(2):237–250. <https://doi.org/10.1016/j.ijrmms.2004.08.008>
- Bieniawski ZT (1967) Mechanism of brittle fracture of rock: part I-theory of the fracture process. *Int J Rock Mech Min* 4(4):395–406. [https://doi.org/10.1016/0148-9062\(67\)90030-7](https://doi.org/10.1016/0148-9062(67)90030-7)
- Chen XD, Wang JJ, Li ZY, Dai F, Wei MD (2021) Experimental investigation of mechanical damage and acoustic emission characteristics of tuff under triaxial compression. *Arab J Geosci* 14(23):138. <https://doi.org/10.1007/s12517-021-08711-x>
- Falmagne V, Kaiser PK, Martin CD (1998) Microseismic monitoring and rock mass degradation. Proceedings of the 100th Canadian Institute of Mining and Metallurgy annual general meeting, Published in CD-ROM 1–8.
- Fu B, Zhou ZH, Wang HQ, Wang YX (2016) Precursor information study on acoustic emission characteristics of marble under uniaxial cyclic loading-unloading. *J China Coal Soc* 41(8):1946–1953. <https://doi.org/10.13225/j.cnki.jccs.2016.0345> (in Chinese)
- Gao YH, Feng XT (2019) Study on damage evolution of intact and jointed marble subjected to cyclic true triaxial loading. *Eng Fract Mech* 215:224–234. <https://doi.org/10.1016/j.engfracmech.2019.05.011>
- Guo HJ, Ji M, Zhang YD, Zhang M (2018) Study of mechanical property of rock under uniaxial cyclic loading and unloading. *Adv Civ Eng* ID:1670180. <https://doi.org/10.1155/2018/1670180>
- Heap MJ, Vinciguerra S, Meredith PG (2009) The evolution of elastic moduli with increasing crack damage during cyclic stressing of a basalt from Mt. Etna volcano. *Tectonophysics* 471(1–2):153–160. <https://doi.org/10.1016/j.tecto.2008.10.004>
- Li T, Pei X, Wang D, Huang R, Tang H (2019) Nonlinear behavior and damage model for fractured rock under cyclic loading based on energy dissipation principle. *Eng Fract Mech* 206:330–341. <https://doi.org/10.1016/j.engfracmech.2018.12.010>
- Liu XS, Ning JG, Tan YL, Gu QH (2016) Damage constitutive model based on energy dissipation for intact rock subjected to cyclic loading. *Int J Rock Mech Min* 85:27–32. <https://doi.org/10.1016/j.ijrmms.2016.03.003>
- Liu XH, Hao QJ, Hu AK, Zheng Y (2020) Study on determination of uniaxial characteristic stress of coal rock under quasi-static strain rate. *Chinese J Rock. Mech Eng* 39(10):2038–2046. <https://doi.org/10.13722/j.cnki.jrme.2020.0321> (in Chinese)
- Manogharan P, Wood C, Marone C, Elsworth D, Riviere J, Shokouhi P (2021) Nonlinear elastodynamic behavior of intact and fractured rock under in-situ stress and saturation conditions. *J Mech Phys Solids* 153:104491. <https://doi.org/10.1016/j.jmps.2021.104491>
- Meng QB, Wang CK, Huang BX, Pu H, Zhang ZT, Sun W, Wang J (2020) Rock energy evolution and distribution law under triaxial cyclic loading and unloading conditions. *Chinese J Rock. Mech Eng* 39(10):2047–2059. <https://doi.org/10.13722/j.cnki.jrme.2020.0208> (in Chinese)
- Meng QB, Zhang MW, Han LJ, Pu H, Chen YL (2018) Acoustic emission characteristics of red sandstone specimens under uniaxial cyclic loading and unloading compression. *Rock Mech Rock Eng* 51(4):968–988
- Meng QB, Zhang MW, Han LJ, Pu H, Nie TY (2016) Effects of acoustic emission and energy evolution of rock specimens under the uniaxial cyclic loading and unloading compression. *Rock Mech Rock Eng* 48:3873–3886. <https://doi.org/10.1007/s00603-016-1077-y>
- Miao SJ, Liu ZJ, Zhao XG, Huang ZJ (2021) Characteristics of energy dissipation and damage of Beishan granite under cyclic loading and unloading. *Chinese J Rock. Mech Eng* 40(05):928–938. <https://doi.org/10.13722/j.cnki.jrme.2020.0953> (in Chinese)
- Mikhalyuk AV, Zakharov VV (1997) Dissipation of dynamic loading energy in quasi-elastic deformation processes in rocks. *J Appl Mech Tech Ph+* 38(2):312–318. <https://doi.org/10.1007/BF02467918>
- Shen WB, Yu WJ, Pan B, Li K (2022) Rock mechanical failure characteristics and energy evolution analysis of coal-rock combination with different dip angles. *Arab J Geosci* 15(1):93. <https://doi.org/10.1007/s12517-021-09268-5>
- Singh TN, Naidu AS (2001) Influence of strain rate and cyclic compression on physico-mechanical behaviour of rock. *Indian J Eng Mater S* 8(1):8–12
- Song SL, Liu XS, Tan YL, Fan DY (2020) Study on failure modes and energy evolution of coal-rock combination under cyclic loading. *Shock Vib* 5:1–16. <https://doi.org/10.1155/2020/5731721>
- Sujathal V, Kishen JMC (2003) Energy release rate due to friction at bimaterial interface in dams. *J Eng Mech* 129(7):793–800. [https://doi.org/10.1061/\(asce\)0733-9399\(2003\)129:7\(793\)](https://doi.org/10.1061/(asce)0733-9399(2003)129:7(793))
- Tang JH, Chen XD, Dai F (2020a) Experimental study on the crack propagation and acoustic emission characteristics of notched rock beams under post-peak cyclic loading. *Eng Fract Mech* 226. <https://doi.org/10.1016/j.engfracmech.2020.106890>
- Tang JH, Chen XD, Dai F, Wei MD (2020b) Experimental investigation of fracture damage of notched granite beams under cyclic loading using DIC and AE techniques. *Fatigue Fract Eng M* 43(7):1583–1596. <https://doi.org/10.1111/ffe.13253>
- Thompson BD, Young RP, Lockner DA (2006) Fracture in westerly granite under AE feedback and constant strain rate loading: nucleation, quasi-static propagation, and the transition to unstable fracture propagation. *pageoph* 163 (5–6):995–1019. 10.1007/s00024-006-0054-x
- Trippetta F, Colletini C, Meredith PG, Vinciguerra S (2013) Evolution of the elastic moduli of seismogenic Triassic evaporites subjected to cyclic stressing. *Tectonophysics* 592:67–79. <https://doi.org/10.1016/j.tecto.2013.02.011>
- Vaneghi RG, Thoeni K, Dyskin AV, Sharifzadeh M, Sarmadivaleh M (2020) Strength and damage response of sandstone and granodiorite under different loading conditions of multistage uniaxial cyclic compression. *Int J Geomech* 20(9):04020159. [https://doi.org/10.1061/\(ASCE\)GM.1943-5622.0001801](https://doi.org/10.1061/(ASCE)GM.1943-5622.0001801)
- Wang JJ, Chen XD, Wei MD, Dai F (2021a) Triaxial fatigue behavior and acoustic emission characteristics of saturated tuff. *Int J Geomech* 21(12):04021230. [https://doi.org/10.1061/\(ASCE\)GM.1943-5622.0002212](https://doi.org/10.1061/(ASCE)GM.1943-5622.0002212)
- Wang Y, Yi YF, Li CH, Han JQ (2021b) Anisotropic fracture and energy characteristics of a Tibet marble exposed to multi-level constant-amplitude (MLCA) cyclic loads: A lab-scale testing. *Eng Fract Mech* 244:107550. <https://doi.org/10.1016/j.engfracmech.2021.107550>

- Wang ZC, Li SC, Qiao LP, Zhao JG (2013) Fatigue behavior of granite subjected to cyclic loading under triaxial compression condition. *Rock Mech Rock Eng* 46(6):1603–1615. <https://doi.org/10.1007/s00603-013-0387-6>
- Wei MD, Dai F, Liu Y, Li A, Yan ZL (2021) Influences of loading method and notch type on rock fracture toughness measurements: from the perspectives of T-stress and fracture process zone. *Rock Mech Rock Eng* 54(9):4965–4986. <https://doi.org/10.1007/s00603-021-02541-9>
- Wu ZH, Song ZY, Tan J, Zhang YZ, Qi ZJ (2020) The evolution law of rock energy under different graded cyclic loading and unloading modes. *J Min Safe Eng* 37(4):836–844+851. <https://doi.org/10.13545/j.cnki.jmse.2020.04.23> (in Chinese)
- Xie HP, Ju Y, Li LY, Peng RD (2008) Energy mechanism of deformation and failure of rock masses. *Chinese J Rock Mech Eng* 27(9):1729–1740 (in Chinese)
- Xu J, Wang WZ, Yang XG, Wang H (2004) Experimental study on the deformation characteristics of fine-sandstone under the loading and unloading conditions. *J Chongqing Uni (NSE)* 27(12):60–62 (in Chinese)
- Zhang MW, Meng QB, Liu SD (2017) Energy evolution characteristics and distribution laws of rock materials under triaxial cyclic loading and unloading compression. *Adv Mater Sci Eng* 8:1–16. <https://doi.org/10.1155/2017/5471571>
- Zhang MW, Meng QB, Liu SD, Qian DY (2018) Impacts of cyclic loading and unloading rates on acoustic emission evolution and felicity effect of instable rock mass. *Adv Mater Sci Eng* ID:8365396. <https://doi.org/10.1155/2018/8365396>
- Zhao K, Yang DX, Gong C, Zhuo YL, Wang XJ (2020) Evaluation of internal microcrack evolution in red sandstone based on time–frequency domain characteristics of acoustic emission signals. *Constr Build Mater* 260. <https://doi.org/10.1016/j.conbuildmat.2020.120435>
- Zhu XJ, Li YY, Wang CX, Sun XZ, Liu ZX (2018) Deformation failure characteristics and loading rate effect of sandstone under uniaxial cyclic loading and unloading. *Geotech Geol Eng* 37:1147–1154. <https://doi.org/10.1007/s10706-018-0674-9>
- Zhu ZH, Feng T, Gong FQ, Ye ZY, Yu Z (2016) Experimental research of mechanical properties on grading cycle loading-unloading behavior of coal-rock combination bodies at different stress levels. *J Cent South Univ (Sci & Tech)* 47(07):2469–2475. <https://doi.org/10.11817/j.issn.1672-7207.2016.07.039> (in Chinese)